Distribution Agreement

In presenting this thesis as a partial fulfillment of the requirements for a degree from Emory University, I hereby grant to Emory University and its agents the non-exclusive license to archive, make accessible, and display my thesis in whole or in part in all forms of media, now or hereafter now, including display on the World Wide Web. I understand that I may select some access restrictions as part of the online submission of this thesis. I retain all ownership rights to the copyright of the thesis. I also retain the right to use in future works (such as articles or books) all or part of this thesis.

Ashley Kim April 10, 2024

Seeding of synthetic amyloid-β(1-42) monomers by amyloid-β(1-42) present in Alzheimer's brains

by

Ashley Kim

David Lynn

Adviser

Department of Chemistry

David Lynn

Adviser

Zhexing Wen

Committee Member

Fang Liu

Committee Member

2024

Seeding of synthetic amyloid-β(1-42) monomers by amyloid-β(1-42) present in Alzheimer's brains

by

Ashley Kim

David Lynn

Adviser

An abstract of
a thesis submitted to the Faculty of Emory College of Arts and Sciences
of Emory University in partial fulfillment
of the requirements of the degree of
Bachelor of Science with Honors

Department of Chemistry

2024

Abstract

Seeding of synthetic amyloid-β(1-42) monomers by amyloid-β(1-42) present in Alzheimer's brains

by Ashley Kim

As aggregates of the self-assembling amyloid-beta(1-42) peptide (Aβ42) become increasingly popular targets in the search for Alzheimer's disease (AD) therapeutics, it is especially critical to further understand the aggregation mechanism and characterize the resulting three-dimensional structures. Prior studies have semi-selectively extracted Aβ42 aggregates out of brain samples from AD patients and characterized them with negative staining and cryo-EM. Helical Aβ42 fibrils can be identified, but the smaller oligomers that are believed to be the toxic agents remain elusive. In this work, we aim to investigate the oligomerization and subsequent fibrillization of Aβ42 in correlation to disease by releasing synthetic rhodamine-labeled Aβ42 (Rho-Aβ42) monomers into AD brain extract. The solid-state monomers were dissolved into brain extract and co-incubated over a 1-day period, theoretically allowing for co-aggregation to occur between synthetic and natural Aβ42 where pre-existing Aβ42 fibrils serve as "seeds" for Rho-Aβ42 addition. Rho-Aβ42 was incubated in both "slow"-progressing and "rapid"-progressing AD extract, along with a neutral salt buffer containing no brain matter. All samples were examined at three time-points (t=0 hr, 3 hr, 24 hr) by negative stain transmission electron microscopy. We found notable differences between the structures of Aβ42 fibrils formed in buffer and brain extract conditions, emphasizing the need to consider the role of other brain components in aggregation regardless of self-assembling properties. Subsequent studies will aim to track the synthetic Aβ42 monomers during their incorporation into brain aggregates using fluorescence microscopy, as they were synthesized with N-terminal Rhodamine B tags.

Seeding of synthetic amyloid-β(1-42) monomers by amyloid-β(1-42) present in Alzheimer's brains

by

Ashley Kim

David Lynn

Adviser

A thesis submitted to the Faculty of Emory College of Arts and Sciences
of Emory University in partial fulfillment
of the requirements of the degree of
Bachelor of Science with Honors

Department of Chemistry

2024

Acknowledgements

I would like to acknowledge my adviser, Dr. David Lynn, as well as fellow members of the Lynn Lab for their continuous support and guidance. I also acknowledge my committee members Dr. Zhexing Wen and Dr. Fang Liu for their assistance in advising this project. A special thanks to John Blankenhorn and the Liang Lab for their collaborative efforts to make this project possible.

This study was supported by Emory University Robert P. Apkarian Integrated Electron Microscopy Core Facility (RRID: SCR_023537), which is subsidized by the School of Medicine and Emory College of Arts and Sciences. Additional support was provided by the Georgia Clinical & Translational Science Alliance of the National Institutes of Health under award number UL1TR000454. The content is solely the responsibility of the authors and does not necessarily reflect the official views of the National Institutes of Health.

Table of Contents

Introduction……..1

Background……..5

Methods……..10

Results……12

Discussion……..18

References……..24

Introduction

Currently, there are at least 50 million people worldwide living with Alzheimer's disease (AD)[1], a devastating neurodegenerative condition that made a dent in the U.S. economy worth 321 billion dollars in 2022 alone[2]. Despite the extensive funding and research efforts that are constantly poured into solving the mystery of AD, it is still untreatable and the progression of the disease is inevitable once detected. The earliest drug approvals by the FDA consisted of symptom management therapies only[3], and advancement in the search for therapeutic strategies that instead impact the disease progression has been significantly slower. Most recently, in 2023, the FDA approved the first two AD treatments that are proven to interfere with progression and delay cognitive decline[4]. These drugs (lecanemab and aducanumab) are disease-modifying therapies known as anti-amyloid monoclonal antibodies[5], meaning that they significantly reduce cognitive decline by specifically targeting and removing amyloid plaques in AD brains[6, 7]. The approval of these anti-amyloid drugs provides promising support for the highly debated "amyloid cascade hypothesis"[8] (ACH), which is a proposal for the underlying mechanisms behind AD pathogenesis that identifies aggregates of amyloid peptides as the main culprits involved in disease initiation and propagation.

The amyloid plaques that are recognized as hallmarks of AD brains[9] are made up of accumulated deposits of amyloid-beta (Aβ) peptides, which are first introduced in the brain as soluble monomers from proteolytic cleavage of the amyloid-β precursor protein (APP)[10]. Several amyloidogenic peptide variants can result from proteolytic cleavage of APP, and the main forms of Aβ in humans are Aβ(1-40) and Aβ(1-42), denoted as Aβ40 and Aβ42 respectively. Although

the two peptides differ only by two residues, Aβ42 is the species found to be most relevant in AD etiology[11].

Prior to the recent discoveries of anti-amyloid treatments, evidence from various approaches have pointed to some degree of correlation between Aβ42 and AD. Firstly, it was recognized that amyloid plaques appeared in greater quantities in diseased brains, and morphological differences were observed in these plaques when compared to those in unaffected brains[9]. In addition to the recognition of differences in accumulated Aβ42 between AD and non-AD patients, studies measuring monomeric Aβ42 have also revealed contrasting levels between the two groups. Specifically, it was observed that Aβ42 concentration in the cerebrospinal fluid (CSF) was lower in disease states[12, 13]. These findings call for further investigation into the decreased CSF Aβ42 concentration. When monomeric Aβ42 is first cleaved off from APP in the interstitial fluid (ISF) of the human brain, there are a number of possibilities for its fate. It could be degraded by proteases[14, 15] or taken up by microglial cells[16] before any migration can occur. Otherwise, it can be transported to be cleared either across the blood-brain-barrier[17] or into the CSF[18]. Thus, if there are fewer Aβ42 monomers in the CSF, it can be concluded that there is some form of inhibition of ISF to CSF transport. The exact route taken by Aβ42 between the two regions is still unclear, indications that this transport is passive imply that only small solutes can access this pathway[19]. Accordingly, an apt explanation for the inhibition would be that the Aβ42 monomers in the ISF assembled into large aggregates that are no longer soluble, preventing clearance into the CSF. If so, then the results of these clinical studies firmly support the direct involvement of Aβ42 aggregation in AD etiology.

The clinical evidence that has been described represents only one side of the supporting arguments, and other compelling information can be found in studying Aβ42 out of the context of AD. The peptide has garnered much attention for its self-assembling properties, revealed through *in vitro* experiments that show the concentration-dependent spontaneous aggregation of Aβ42 monomers in solution[20]. In the process of assembly, Aβ42 monomers first nucleate to form smaller soluble aggregates before continuing to elongate into long, helical fibrils[21]. However, it is important to note that progression to fibrillation does not always occur, and aggregates may remain in relatively stable oligomer or protofibril products[22]. The underlying kinetic pathways behind these conformational transitions are particularly difficult to elucidate due to the reversible equilibrium between monomers and fibrils that results in dynamic polymorphs[23, 24]. To find connections between Aβ42 aggregation and disease, previous studies have aimed to correlate the presence of Aβ42 polymorphs and toxicity to neurons[25]. Several of these reports support the notion that the primary toxicity-inducing species are the oligomeric "intermediates" between monomers and fibrils, characterized by their mysterious lack of defined structure and metastability[26, 27]. The overarching concept of the ACH involves a prion-like consideration of these toxic oligomers[8, 28], which suggests that AD is initiated by Aβ42 oligomerization and spread through oligomer self-propagation[29]. This implies that toxic aggregate conformations are achieved only through specific kinetic pathways, so identifying a connection between distinct Aβ42 aggregation pathways and disease states would provide compelling evidence in support of the hypothesis.

Therefore, in this project, the overarching strategy to identify this connection is to amplify the proposed toxic Aβ42 species and observe a hypothesized amplification of AD propagation as a

result. In order to template the formation of more toxic Aβ42 polymorphs from those that we propose to exist as propagators in AD brains, we employ synthetic fluorescently-labeled Aβ42 monomers and "seed" them into brain extract. Using the fluorescent tag, we aim to probe the assembly process of added monomers which we hypothesize to be catalyzed by existing Aβ42 species. To observe the effect of this seeding on disease propagation, we utilize the recent identification of genotypic markers that correlate to the degree of propagation. Specifically, two phenotypic clusters of "rapid" and "slow" progressing disease have been identified and corresponding differential gene expression was subsequently discovered*. Thus, we propose that upon future studies in cortical organoids to simulate biological activity, we will observe the differential gene expression associated with greater propagation rates upon the seeding of synthetic monomers. In this preliminary study, we aim to establish proof of principle that brain-derived Aβ42 able to seed fluorescently tagged synthetic monomers and make initial qualitative observations through imaging as a basis for subsequent experimental design.

* Gordon-Kim, C.; Xu, C.; Li, N.X.; Poppitz, G.; Veinbachs, E.; Pidugu, A.; Niu, W.; Walker, L.C.; Wen, Z.; Lynn, D.G. **2023** (in preparation)

Background

Proposed aggregation pathways

The pathways taken by Aβ42 monomers to assemble into higher-order polymorphs are not well-understood at this time, but structural and kinetic studies have shed light onto the process. In particular, thioflavin T (ThT) fluorescence experiments are a common approach to studying the kinetics of Aβ42 monomers in solution as fibrillar species display an increased quantum fluorescence yield[30]. The ThT fluorescence over time of incubated Aβ42 monomers takes on a sigmoidal curve representing the conformational transition of the main species in solution[31]. Rapid oligomerization is seen among monomers, and the concentration of monomers and low-molecular-weight oligomers decreases over time as the dominant species becomes large fibrils[32]. It is important to note that many polymorphs of aggregated Aβ42 are simultaneously present in solution, and these forms can be categorized as soluble (monomer, oligomer) and insoluble (protofibril, fibril). The structures of the smaller oligomers are obscure, while the protofibrils possess more defined, nodular structures that serve as precursors to mature fibrils[33].

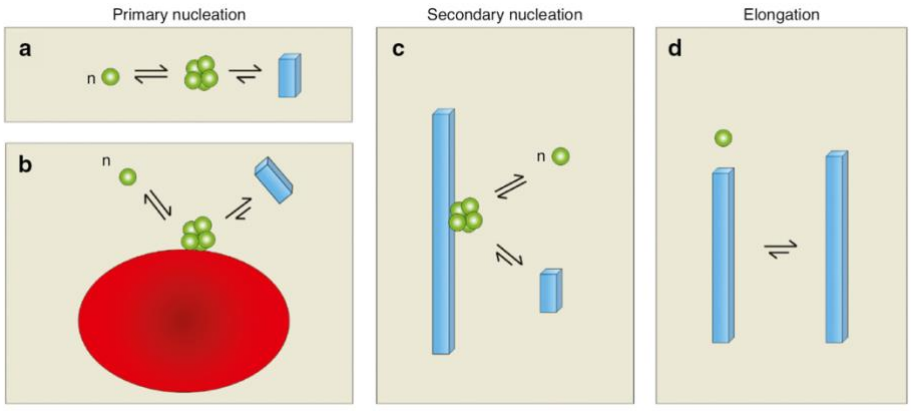

Figure 1[35]. Schematic depicting the proposed aggregation pathway for Aβ42. (a) Homogeneous primary nucleation involves monomers forming a nucleating core prior to fibril formation (b) Heterogeneous primary nucleation, where nucleation occurs on a foreign surface (c) Secondary nucleation involves monomers nucleating on the surface of a pre-existing fibril to form new fibrils (d) Elongation involves the addition of monomers to growing fibrils

It is highly supported that Aβ42 monomers undergo a nucleation-dependent mechanism that is determined by either "primary" or "secondary" nucleation to achieve larger structures[34] (Fig. 1). In the primary nucleation event, free monomers aggregate to form an oligomeric nucleus that acts as a core for further monomer addition. In the secondary nucleation event, the nucleating core is not formed from free monomers, but rather, pre-aggregated forms of Aβ42. That is, Aβ42 monomers can nucleate along the surface of previously formed mature fibrils of Aβ42. In this case, the pre-existing Aβ42 fibrils are known as "seeds" for added monomers. After the rate-limiting nucleation step, the elongation step begins to grow aggregates into mature fibrils, and these steps have been shown to be thermodynamically distinct[35].

Understanding Aβ42 aggregation through its primary sequence

As with any amino acid construct, the conformations of Aβ42 are ultimately determined by its primary sequence at the root. The native primary sequence of Aβ42 is:

DAEFRHDSGYEVHHQKLVFFAEDVGSNKGAIIGLMVGGVVIA.

The 42-residue chain is widely considered as four functionally distinct segments consisting of the N-terminal metal-binding region ($A\beta_{1-16}$), the C-terminal hydrophobic region ($A\beta_{30-42}$), and the two central regions: the hydrophobic core ($A\beta_{17-21}$) and the polar region ($A\beta_{22-29}$) (Fig. 2). In general, the high content of hydrophobic side chains in Aβ42 is well-known to be largely responsible for its amyloidogenicity, especially because it is more hydrophobic than other Aβ variants that are less prone to aggregation[36]. This has been supported by various experimental approaches, including thermodynamic considerations, mutagenesis to alter hydrophobicity, and structural observations. One of the most fascinating discoveries about the hydrophobic regions of the sequence is the "hydrophobic ladder" model that rationalizes the three-dimensional

architecture of Aβ42 filaments[37]. The repeated pattern that is observed in these helical filaments is known as the cross-beta structure[38], which is commonly seen in other insoluble peptide aggregates as well[39]. In this structure, the repeated unit consists of two monomers in a laminated pair of parallel, in-register beta sheets, where each monomer demonstrates a beta strand - turn - beta strand motif from residues 18 to 42[40]. Note that this region begins and ends with each hydrophobic core, so the turn between them allows for the ladder-like structure where the hydrophobic regions are the rungs.

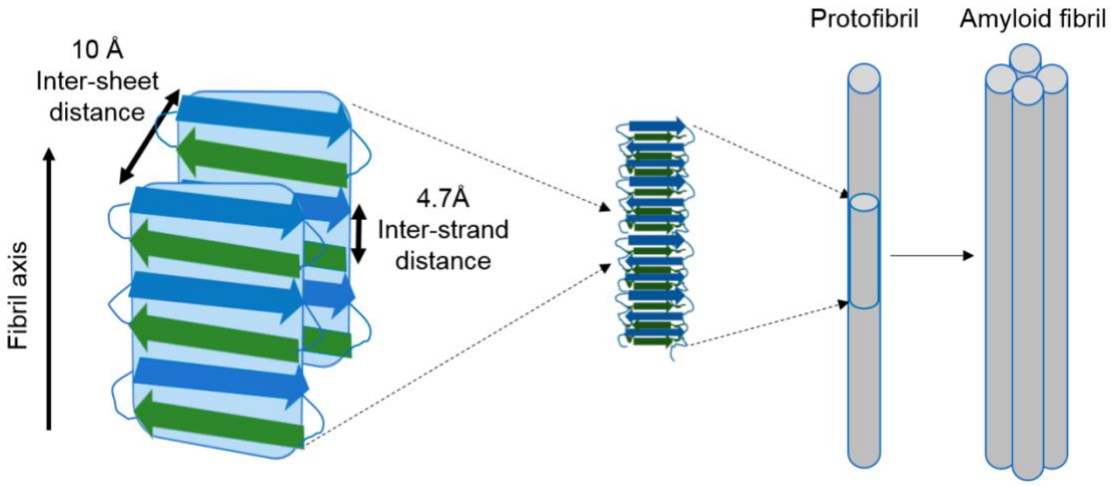

Figure 2[38]. Schematic depicting the cross-beta architecture, where the green and blue arrows depict beta strands

Experiments with mutated variants of Aβ42 have confirmed that the hydrophilic regions of the sequence are somehow involved in folding as well, but it has proven to be more difficult to demonstrate functions of these regions in direct relation to aggregation and the disease state. A key discovery that relates the electrostatic interactions of Aβ42's residues to aggregation is the highly sensitive pH dependence of oligomerization observed *in vitro.* Over the years, researchers have arrived at a general agreement that the aggregation of Aβ42 is promoted by acidic conditions, and interestingly, it has been found that the only part of aggregation that is affected

by pH is the primary nucleation[41]. Additional studies on the individual-residue level have revealed the effects of protonation/deprotonation or ion bridging at certain positions[42], and these findings have allowed for the generation of new theories and models of the aggregation pathway.

While intermolecular electrostatic interactions between peptides are certainly important for aggregation, another ionic consideration lies in the metal-binding properties of Aβ42. The well-known prevalence of metal ions in neurological processes implies their presence in the Aβ42 aggregation environment of the human brain. Metal binding alters the stability of certain conformational states, so these complexes display modulated kinetics during aggregation which lead to variations in the expected equilibrium ratios of monomers, oligomers, and higher-order polymeric states such as filaments[43]. Given the evidence that proves the toxicity of Aβ42 aggregates is dependent on its degree of assembly[27], this suggests that metal ions could potentially contribute to Aβ42's role in disease. It has been found that Aβ42 is able to complex several transition metals *in vitro*[44], and in particular, interactions with Cu(II) and Zn(II) ions have been extensively studied because of their relevance in the brain chemistry where Aβ42 is found. These ions each have distinct effects on aggregation mechanisms, but the most striking difference between them may be their redox potentials. Unlike Aβ42-Zn(II) complexes, Aβ42-Cu(II) complexes are able to undergo redox cycling, which generates reactive oxygen species[45]. Oxidative stress is known to promote neuron death, so some believe that the Cu(II) ion has a key role in AD and efforts to treat the disease with metal chelation therapy have been initiated[46]. The drastic differences in behavior between pure Aβ42 structures and corresponding metal complexes serve as a reminder that external species can significantly impact the aggregation pathway and should absolutely be considered in these studies.

"Slow" and "rapid" progressing Alzheimer's disease

Statistical analysis of AD progression in human subjects has revealed two distinct sub-categories of the disease: "slow" and "rapid" progressing[47]. The terms "slow" and "rapid" refer to the rate at which mild cognitive impairment (MCI) evolves into dementia. Additional statistical studies have shown that if a patient begins experiencing AD progression under one of these categories, the disease will continue to progress at that rate for its entirety[48]. This evidence supports the idea that the pathways behind the pathogenesis may be completely different for the two categories, yet the underlying factors responsible for the contrasting mechanisms have yet to be identified. Several biomarkers in the brain believed to be correlated with AD have been compared between the two categories, and a significant difference in the amount of Aβ42 in the cerebrospinal fluid (CSF) was discovered. Specifically, AD patients under the "slow" category had a significantly higher concentration of Aβ42 in the CSF than those under the "rapid" category[47]. It is important to mention that notable differences were found in other biomarkers as well, but nonetheless, this finding raises new perspectives on the amyloid cascade hypothesis. Because of the dynamic polymorphism of Aβ42 oligomers and their sensitive tunability, it is possible that different modes of aggregation relate to different modes of disease progression. The mystery that lies behind these distinguishable variations of AD poses yet another question that calls for further exploration of Aβ42 aggregation.

Methods

Extraction of Aβ42 from patient-derived brain samples

Brain samples derived from deceased AD patients were provided by the Alzheimer's Disease Research Center (ADRC). Each sample is identified by a number corresponding to a unique patient and categorized by "slow" or "rapid" progressing AD. Semi-specific extraction Aβ42 was performed on two samples in this study: "slow" sample 14-88 and "rapid" sample 14-14. A portion of each brain sample weighing approximately 0.5 g was cleaved from the provided amount and homogenized into an extraction buffer (10 mM Tris-HCl, pH 7.4, 0.8 M NaCl, 10% sucrose, 1 mM EGTA). The homogenate was brought to 2% sarkosyl (w/v) by addition of 10% sarkosyl (w/v) stock solution and left to incubate at 37°C for 60 minutes. Following incubation, the homogenate underwent a 10 min centrifugation at 10,000 g to form a pellet. The pellet was discarded while the supernatant underwent a 60 min centrifugation at 100,000 g to form another pellet. The supernatant was then discarded while the pellet was resuspended in the extraction buffer before being centrifuged for 10 min at 3,000 g. The resulting supernatant was diluted 3-fold in a buffer of 20 mM Tris-HCl, pH 7.4, 0.15 M NaCl, 10% sucrose, 0.2% sarkosyl and centrifuged for 30 min at 100,000 g. The resulting pellet was resuspended in a buffer of 20 mM Tris-HCl, pH 7.4, 50 mM NaCl then centrifuged for 2 min at 3,000 g. The pellet was discarded, and the supernatant was incubated with 0.4 mg/mL of pronase for 45 minutes at 37°C to complete the extraction.

Co-incubation of synthetic Aβ42 and brain extract

Synthetic Aβ42 peptide labeled with Rhodamine B at the N-terminus (Rho-DAEFRHDSGYEVHHQKLVFFAEDVGSNKGAIIGLMVGGVVIA) in solid, monomeric form was purchased from LE Biochem CO., Ltd. The synthetic Aβ42 was dissolved in the following experimental conditions: "slow" sample 14-88 extract, "rapid" sample 14-14 extract, and buffer (20 mM Tris-HCl, pH 7.4, 50 mM NaCl). The mass of synthetic Aβ42 added to brain extract was calculated to satisfy a 20:1 ratio of synthetic Aβ42 to brain Aβ42 and a total final Aβ42 concentration of 1.0 mg/mL, under the assumption of an Aβ42 concentration of 0.4 mg/mL naturally present in brain extract. Immediately upon dissolution, samples of each solution were removed for the t=0hr time-point. The solutions were then incubated at 37°C and samples were collected at time-points t=3hr, 24hr. All samples were frozen at -80°C between collection and imaging.

Negative stain

Negative stain grids were prepared at each time-point (t=0hr, 3hr, 24 hr) for each of the three solutions (buffer, "slow", "rapid"). In each preparation, carbon-coated TEM grids were first glow discharged for 1 min using the PELCO easiGlow™ cleaning system. Then, each sample was spotted onto a grid and allowed to sit for 1 min before blotting off the excess liquid with blotting paper. After two rounds of dipping the sample-loaded grids into water and blotting off the excess, the grids were stained with uranyl formate solution. After 1 min, the excess uranyl formate solution was blotted off to complete grid preparation. Negative stain images were collected using a ThermoFisher Talos 120 kV transmission electron microscope.

Results

The three samples used in this experiment will be referred to as *buffer* (synthetic Aβ42 + salt buffer), *slow* (synthetic Aβ42 + "slow" progressing AD brain extract), and *rapid* (synthetic Aβ42 + "rapid" progressing AD brain extract). Each of the three samples was imaged at three time-points (t=0hr, 3hr, 24hr), so nine sets of negative stain TEM images were obtained from this experiment.

The images of the t=0hr time-point reflect the samples immediately after they were prepared. Images of *buffer* at t=0hr contained irregularly round dark patches, signifying that some degree of aggregation had occurred between the synthetic Aβ42 monomers in the minutes between the sample preparation and freezing (Fig. 3A). After incubation, at t=3hr, it is clear that further Aβ42 aggregation had occurred (Fig. 3B). Large, irregular masses of peptides were seen throughout the grid, and there appeared to be Aβ42 fibrils sprouting out of some of these masses. At t=24hr, a greater degree of overall aggregation was seen, and clearly identifiable fibrils were present among areas of highly concentrated aggregated masses (Fig. 3C). One image portrayed a peptide aggregate containing circular "holes", which appear to be liquid-like droplets. At this final time-point, some images displayed a large, well-defined band consisting of what appeared to be insoluble particles of synthetic Aβ42. These bands were several orders of magnitude larger than all other structures identified in *buffer*, and it is possible that they were formed on the grid during the staining process. It is important to note that upon completing 24 hours of incubation, the contents of the Eppendorf tube containing *buffer* no longer appeared entirely homogeneous, and

a small precipitate could be seen at the bottom. It is likely that a fraction of synthetic Aβ42 came out of solution over the course of incubation and interfered with grid preparation.

At t=0hr, images of *slow* included what appeared to be aggregates of brain-derived Aβ42 (Fig. 4A). The aggregates were present in branch-like masses, and it is possible to identify the defined shape of Aβ42 fibrils within the larger structures. The fibrils in the aggregate masses were arranged in an overlapping fashion to achieve the branching effect. A high concentration of the blood protein ferritin was apparent throughout the grid, and these molecules are easily identifiable by their circular ring shape containing a concentric dark core made up of the iron in storage[49]. At t=3hr, *slow* appeared to contain more aggregates overall (Fig. 4B), and some of these masses appeared to be significantly larger than those seen at t=0hr. Similarly to the initial images, these aggregates were disordered and still contained the branch-like structure. However, it is notable that the distinct fibril structure could no longer be seen at t=3hr. Again, ferritin molecules were present, but they appeared significantly less concentrated throughout the grid compared to t=0hr. Finally, at t=24hr, images of *slow* appeared to contain a greater number of aggregates, which seemed to show up cloudier and lighter colored on this grid compared to the others (Fig. 4C). While it may have been a consequence of this particular stain, the branching nature was more difficult to distinguish in the aggregates. Instead, the aggregates appeared to consist of rounded concentrated sub-masses of peptide. In the final time-point, another decrease in the concentration of ferritin molecules was observed.

Lastly, for *rapid*, it appeared that the t=0hr negative stain grid was not properly prepared, and it was difficult to distinguish structures from these images (Fig. 5A). Regardless, it was still evident that the sample contained aggregated masses. Similarly to *slow*, images of *rapid* from

t=3hr clearly showed branch-like aggregates and no evidence of fibrils (Fig. 5B). Ferritin molecules can be seen as well. At t=24hr, *rapid* contained Aβ42 fibrils, many of which formed masses by overlapping with each other (Fig. 5C). Ferritin molecules were also present in comparable amounts to t=3hr. The large bands that appeared on the grid for *buffer* at t=24hr were seen again in *rapid* at t=24hr, and insoluble peptide was also observed in this sample post-incubation.

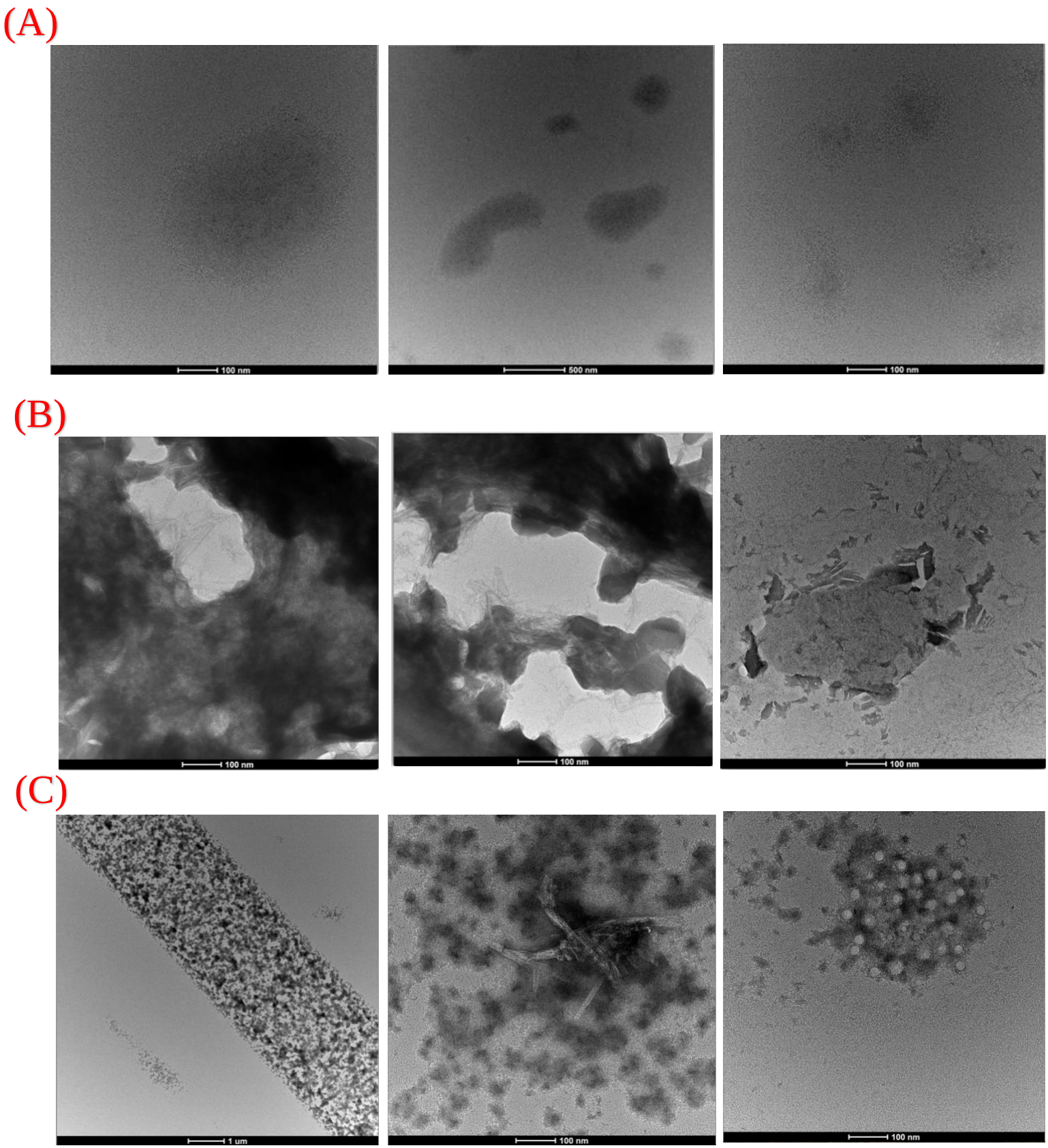

Figure 3. Negative stain transmission electron microscopy images of synthetic Rhodamine B-labeled Aβ42 dissolved in buffer (20 mM Tris-HCl, pH 7.4, 50 mM NaCl) incubated at 37°C for (A) t=0 hours (B) t=3 hours (C) t=24 hours.

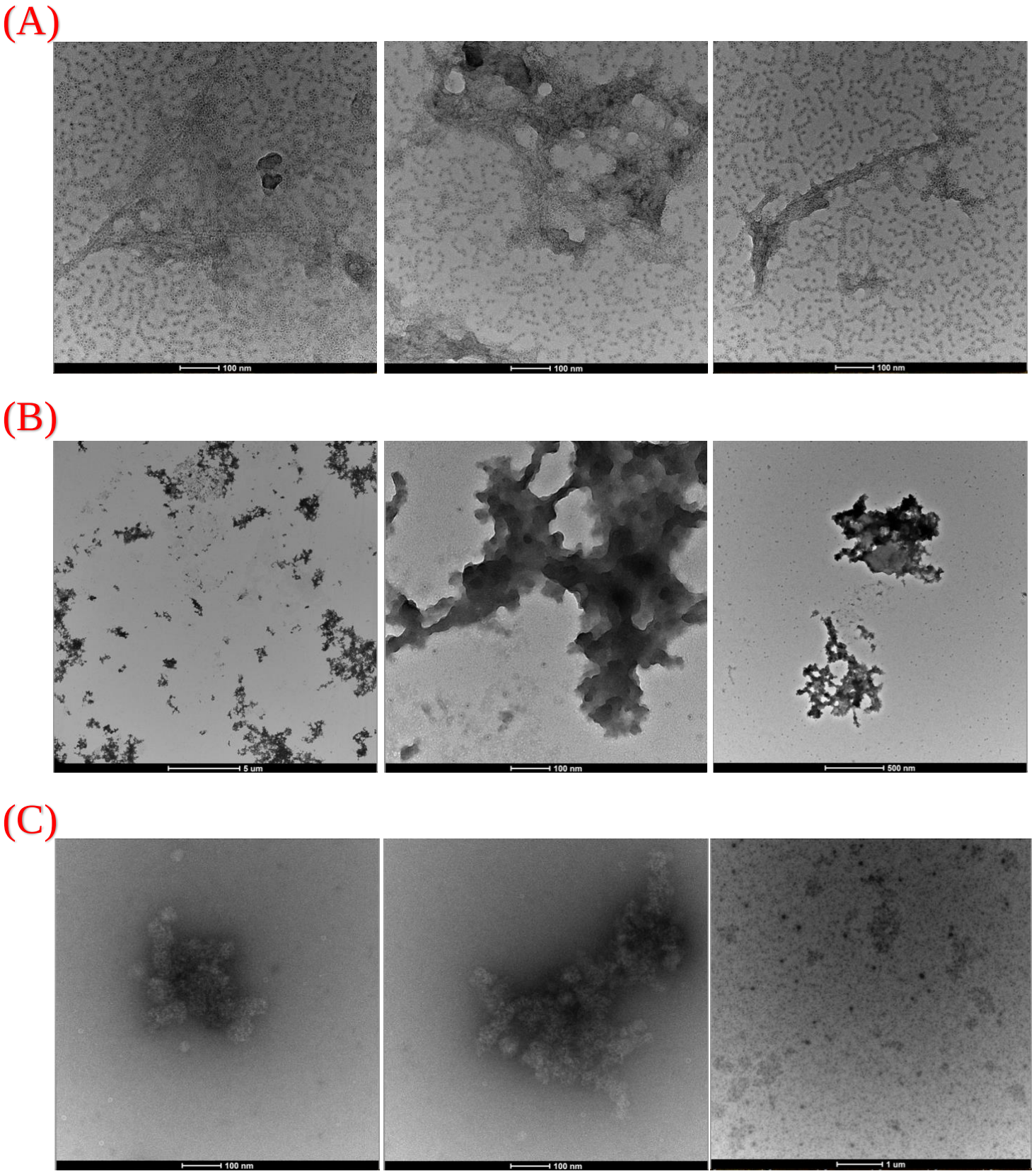

Figure 4. Negative stain transmission electron microscopy images of synthetic Rhodamine B-labeled Aβ42 dissolved in "slow" progressing AD brain extract (sample 14-88) incubated at 37°C for (A) t=0 hours (B) t=3 hours (C) t=24 hours.

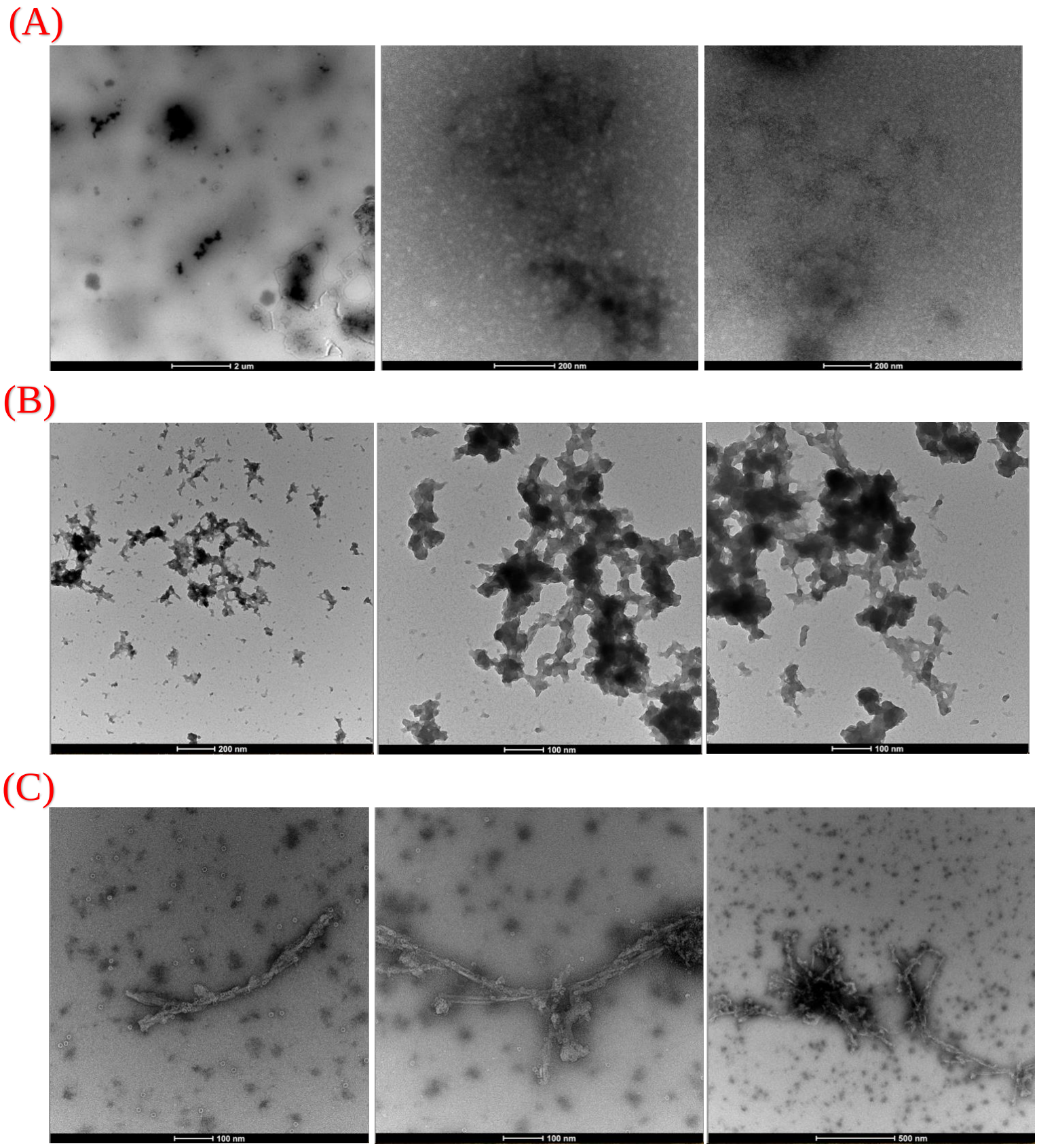

Figure 5. Negative stain transmission electron microscopy images of synthetic Rhodamine B-labeled Aβ42 dissolved in "rapid" progressing AD brain extract (sample 14-14) incubated at 37°C for (A) t=0 hours (B) t=3 hours (C) t=24 hours.

Discussion

This project presents a preliminary starting point for a series of future studies that aims to uncover the aggregation mechanisms of Aβ42 that are responsible for disease. As the first stage in this proposed series, the most valuable conclusions from this experiment lie in the questions raised rather than answered.

A core intention of this experiment was to compare the aggregation of synthetic rhodamine-labeled Aβ42 in the presence and absence of the Aβ42 seeds in brain extract. From the images obtained, there appear to be notable comparisons to be made between the aggregation seen in *buffer* and in the samples containing brain extract. Firstly, we see that the Rho-Aβ42 in *buffer* forms fibrils by the end of the incubation, but they are visibly different from the fibrils that present in brain extract. Prior work by the Liang Lab has resulted in negative stain TEM images of the brain samples used in this experiment without the addition of any synthetic peptide, which serve as controls in this study. In the images of both "slow" (Fig. 6) and "rapid" (Fig. 7) progressing extracts alone, the distinctly helical structure of the Aβ42 fibrils is clearly visible, and the regularly spaced dark spots spanning the fibrils represent their overlap as they twist. In contrast, the fibrils formed by Rho-Aβ42 are wider and do not appear as visibly helical. Although their shape is not as defined in the t=24hr images of *buffer* as it is in the images of extract alone, the fibrils still appear to be twisted. The difference seems to lie in the degree of twisting, also known as the "helical pitch"[50]. While the brain fibrils appear to make at least two or three rotations down each helix, the synthetic fibrils hardly seem to make a full rotation throughout the entire strand.

It is crucial to consider the effect of the Rhodamine B label on the aggregation of Aβ42 when attempting to compare the Rho-Aβ42 experiment with naturally occurring Aβ42. The differences in behavior between labeled and unlabeled synthetic Aβ42 are not well-studied, and the limited evidence that does exist claims that the Rhodamine B label heightens the propensity of Aβ42 monomers to oligomerize[51]. While limitations on materials prevented experiments using unlabeled synthetic Aβ42 monomers at the time of this report, it would be ideal to collect images of those aggregates in the near future as their degree of similarity to Rho-Aβ42 aggregates may affect the validity of the current results.

Aside from the label, there are several other factors that could rationalize the observed differences in Aβ42 fibrils in buffer and in the human brain. Even following an extraction protocol designed to isolate Aβ42 from all brain contents, it is evident from imaging that other species remain. Larger molecules such as ferritin and the lipoprotein APOE have been identified from TEM images of extract, and the brain matter undoubtedly contains a multitude of small solutes that can potentially affect aggregation. For example, it is possible that the Aβ42 fibrils seen in extract are not purely constructed of peptides and may exist as complexes with transition metal ions found in the brain, as metal binding has been shown to impact aggregation[44, 52-54].

One of the most remarkable results from this experiment is the apparent absence of Aβ42 fibrils seen in brain extract following incubation with Rho-Aβ42. Although t=0hr images of *rapid* were unclear as previously mentioned, the t=0hr images of *slow* confirm that fibrils were initially present in the sample. These structures closely resembled previously identified Aβ42 fibrils in the brain that are distinct from the synthetic fibrils observed in *buffer*. Additionally, the *buffer*

experiment agreed with many previous studies on the time dependence of Aβ42 by showing that fibrils are formed over hours[55], not minutes, so it can be concluded with certainty that the fibrils seen in t=0hr *slow* were brain-derived. Additionally, it can be assumed that both *slow* and *rapid* initially contained natural Aβ42 fibrils because the structures were clearly identifiable in negative stain TEM images of the exact extracts used in this project that were previously collected (Fig. 6, 7). However, neither of the extract samples appeared to contain fibrils when images at t=3hr, and no fibrils were found in *slow* at t=24hr as well. Few fibrils could be identified in *rapid* at t=24hr, but there were significantly less than what had been seen in the pure extract. These fibrils were most likely pre-existing natural Aβ42 structures, not formed by Rho-Aβ42 monomers, which was suggested from comparisons to observations of confirmed natural Aβ42 fibrils and synthetic Rho-Aβ42 fibrils. Aside from the mysterious absence of the expected natural Aβ42 fibrils in the images post-incubation, it is also notable that no evidence of synthetic fibril formation was observed either. It is crucial to rationalize the absence of both types of fibrils to follow up on these results.

Firstly, the absence of natural Aβ42 fibrils when expected implies that either they were not visible in the imaged samples or they were no longer present in the samples. It is important to note that these samples were taken from heterogenous solutions and therefore, each sample was not likely to contain an accurate representation of the sample contents as a whole. While there is no evidence of fibril deconstruction upon exposure to excess monomers in solution, it is possible that their distinct structures were somehow disrupted by the seeding. Another explanation would be that they were still present in the samples but no longer visible by electron microscopy. This would be the case if the natural fibrils were somehow obstructed from the camera by another

species, and we hypothesize that the natural fibrils were "coated" by the added Rho-Aβ42 monomers to explain their absence in the t=3hr and t=24hr images. This would be consistent with our initial hypothesis derived from existing evidence that demonstrates the ability of pre-assembled Aβ42 fibrils to seed the aggregation of Aβ42 monomers upon co-incubation *in vitro*[56]. Then, the differences in Aβ42 structures seen between *buffer* and extract samples may be rationalized by the differences between aggregation mechanisms. This idea is also consistent with the lack of synthetic fibrils observed in extract, as the monomers would not be able to undergo fibrillization before being sequestered by the seed fibrils. In order to validate this theory, it is necessary to employ fluorescence microscopy to detect Rho-Aβ42 in the samples and distinguish synthetic Aβ42 from natural Aβ42 using side-by-side comparisons of fluorescence and TEM images. Hence, the process of configuring the TEM grids used for this report to be suitable for fluorescence microscopy has been initiated and this will be the immediate next step in this project.

While the structural information that can be best extracted from these results is mostly about Aβ42 fibrils, it is the Aβ42 oligomers that are primarily known to be most responsible for toxicity. Although these oligomers are difficult to identify with the current results alone, their role as "intermediates" between monomers and fibrils provide a basis for extending these results into future directions. Again, this emphasizes the need for fluorescence studies to be able to positively identify amorphous, ambiguous particles as Aβ42. In conclusion, this study presents a novel approach to deciphering the complex nature of Aβ42 aggregation in relation to AD. We initiated the process towards the eventual goal of tracking Aβ42 aggregation pathways in

diseased brains by conducting preliminary seeding experiments using synthetic Rho-Aβ42 monomers and AD brain extract containing natural Aβ42 fibrils.

It is evident from the obtained images that the aggregation of synthetic Rho-Aβ42 is qualitatively distinct between AD brain and buffer conditions. Most notably, while Rho-Aβ42 fibrils could be observed after incubation in buffer, no fibrils could be identified in the brain samples. Additionally, the addition of synthetic Rho-Aβ42 to brain Aβ42 fibrils resulted in new morphologies that were not previously seen in brain extract alone. These findings support the idea that seed-catalyzed secondary nucleation is a distinct mechanistic step through which toxic Aβ42 structures are formed, opening the doors to subsequent fluorescence experiments that have the potential to validate this argument.

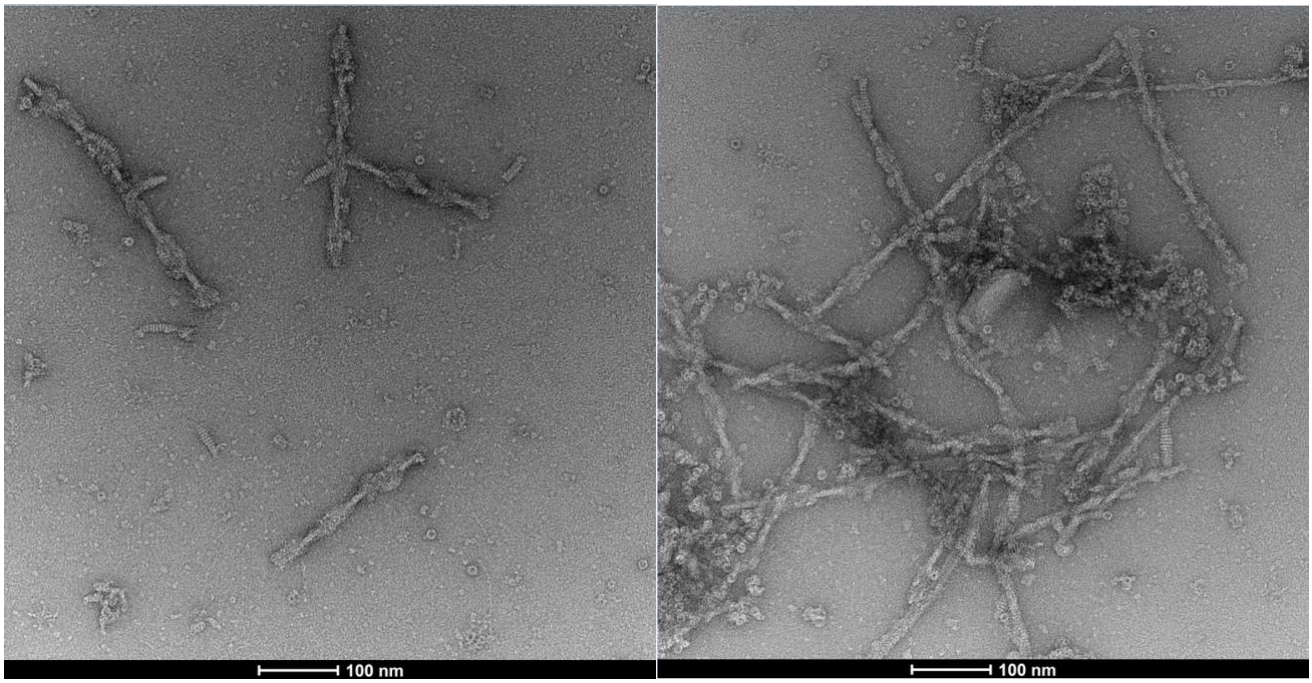

Figure 6. Negative stain transmission electron microscopy images of “slow” progressing AD brain extract (sample 14-88) alone

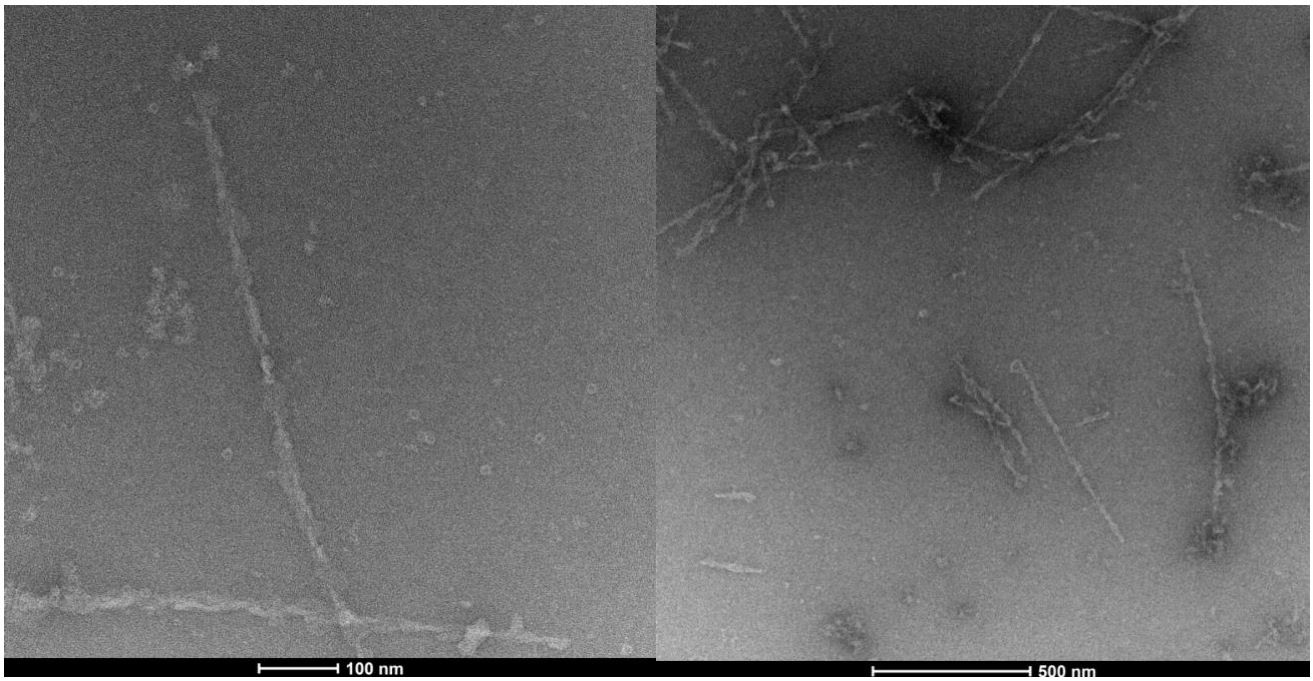

Figure 7. Negative stain transmission electron microscopy images of “rapid” progressing AD brain extract (sample 14-14) alone

References

(1) Breijyeh, Z.; Karaman, R. Comprehensive Review on Alzheimer's Disease: Causes and Treatment. *Molecules* **2020**, *25* (24), 5789.

(2) The Economic Costs of Alzheimer's Disease. In *Joint Economic Committee*, Joint Economic Committee: YouTube, 2022.

(3) Melnikova, I. Therapies for Alzheimer's disease. *Nature Reviews Drug Discovery* **2007**, *6* (5), 341-342. DOI: 10.1038/nrd2314.

(4) Wu, W.; Ji, Y.; Wang, Z.; Wu, X.; Li, J.; Gu, F.; Chen, Z.; Wang, Z. The FDA-approved anti-amyloid-β monoclonal antibodies for the treatment of Alzheimer's disease: a systematic review and meta-analysis of randomized controlled trials. *Eur J Med Res* **2023**, *28* (1), 544. DOI: 10.1186/s40001-023-01512-w From NLM.

(5) Cummings, J. Anti-Amyloid Monoclonal Antibodies are Transformative Treatments that Redefine Alzheimer's Disease Therapeutics. *Drugs* **2023**, *83* (7), 569-576. DOI: 10.1007/s40265-023-01858-9.

(6) Sevigny, J.; Chiao, P.; Bussière, T.; Weinreb, P. H.; Williams, L.; Maier, M.; Dunstan, R.; Salloway, S.; Chen, T.; Ling, Y.; et al. The antibody aducanumab reduces Aβ plaques in Alzheimer's disease. *Nature* **2016**, *537* (7618), 50-56. DOI: 10.1038/nature19323.

(7) Walsh, S.; Merrick, R.; Richard, E.; Nurock, S.; Brayne, C. Lecanemab for Alzheimer's disease. *BMJ* **2022**, *379*, o3010. DOI: 10.1136/bmj.o3010.

(8) Fedele, E. Anti-Amyloid Therapies for Alzheimer's Disease and the Amyloid Cascade Hypothesis. *International Journal of Molecular Sciences* **2023**, *24* (19), 14499.

(9) Braak, H.; Braak, E.; Bohl, J.; Lang, W. Alzheimer's disease: amyloid plaques in the cerebellum. *Journal of the Neurological Sciences* **1989**, *93* (2), 277-287. DOI: https://doi.org/10.1016/0022-510X(89)90197-4.

(10) Kang, J.; Lemaire, H. G.; Unterbeck, A.; Salbaum, J. M.; Masters, C. L.; Grzeschik, K. H.; Multhaup, G.; Beyreuther, K.; Müller-Hill, B. The precursor of Alzheimer's disease amyloid A4 protein resembles a cell-surface receptor. *Nature* **1987**, *325* (6106), 733-736. DOI: 10.1038/325733a0 From NLM.

(11) Hansson, O.; Lehmann, S.; Otto, M.; Zetterberg, H.; Lewczuk, P. Advantages and disadvantages of the use of the CSF Amyloid β (Aβ) 42/40 ratio in the diagnosis of Alzheimer's Disease. *Alzheimer's Research & Therapy* **2019**, *11* (1), 34. DOI: 10.1186/s13195-019-0485-0.

(12) Zaretsky, D. V.; Zaretskaia, M. V.; Molkov, Y. I.; for the Alzheimer's Disease Neuroimaging, I. Patients with Alzheimer's disease have an increased removal rate of soluble beta-amyloid-42. *PLOS ONE* **2022**, *17* (10), e0276933. DOI: 10.1371/journal.pone.0276933.

(13) Motter, R.; Vigo-Pelfrey, C.; Kholodenko, D.; Barbour, R.; Johnson-Wood, K.; Galasko, D.; Chang, L.; Miller, B.; Clark, C.; Green, R.; et al. Reduction of beta-amyloid peptide42 in the cerebrospinal fluid of patients with Alzheimer's disease. *Ann Neurol* **1995**, *38* (4), 643-648. DOI: 10.1002/ana.410380413 From NLM.

(14) Miners, J. S.; Barua, N.; Kehoe, P. G.; Gill, S.; Love, S. Aβ-Degrading Enzymes: Potential for Treatment of Alzheimer Disease. *Journal of Neuropathology & Experimental Neurology* **2011**, *70* (11), 944-959. DOI: 10.1097/NEN.0b013e3182345e46 (acccessed 3/29/2024).

(15) Farris, W.; Mansourian, S.; Chang, Y.; Lindsley, L.; Eckman, E. A.; Frosch, M. P.; Eckman, C. B.; Tanzi, R. E.; Selkoe, D. J.; Guénette, S. Insulin-degrading enzyme regulates the levels of insulin, amyloid β-protein, and the β-amyloid precursor protein intracellular domain *in vivo*. *Proceedings of the National Academy of Sciences* **2003**, *100* (7), 4162-4167. DOI: doi:10.1073/pnas.0230450100.

(16) Guan, Y.-H.; Zhang, L.-J.; Wang, S.-Y.; Deng, Y.-D.; Zhou, H.-S.; Chen, D.-Q.; Zhang, L.-C. The role of microglia in Alzheimer's disease and progress of treatment. *Ibrain* **2022**, *8* (1), 37-47. DOI: https://doi.org/10.1002/ibra.12023.

(17) Castellano, J. M.; Deane, R.; Gottesdiener, A. J.; Verghese, P. B.; Stewart, F. R.; West, T.; Paoletti, A. C.; Kasper, T. R.; DeMattos, R. B.; Zlokovic, B. V.; et al. Low-density lipoprotein receptor overexpression enhances the rate of brain-to-blood Aβ clearance in a mouse model of β-amyloidosis. *Proceedings of the National Academy of Sciences* **2012**, *109* (38), 15502-15507. DOI: doi:10.1073/pnas.1206446109.

(18) Iliff, J. J.; Wang, M.; Liao, Y.; Plogg, B. A.; Peng, W.; Gundersen, G. A.; Benveniste, H.; Vates, G. E.; Deane, R.; Goldman, S. A.; et al. A Paravascular Pathway Facilitates CSF Flow Through the Brain Parenchyma and the Clearance of Interstitial Solutes, Including Amyloid β. *Science Translational Medicine* **2012**, *4* (147), 147ra111-147ra111. DOI: doi:10.1126/scitranslmed.3003748.

(19) Deane, R.; Bell, R. D.; Sagare, A.; Zlokovic, B. V. Clearance of amyloid-beta peptide across the blood-brain barrier: implication for therapies in Alzheimer's disease. *CNS Neurol Disord Drug Targets* **2009**, *8* (1), 16-30. DOI: 10.2174/187152709787601867 From NLM.

(20) Novo, M.; Freire, S.; Al-Soufi, W. Critical aggregation concentration for the formation of early Amyloid-β (1–42) oligomers. *Scientific Reports* **2018**, *8* (1), 1783. DOI: 10.1038/s41598-018-19961-3.

(21) Tiiman, A.; Krishtal, J.; Palumaa, P.; Tõugu, V. In vitro fibrillization of Alzheimer's amyloid-β peptide (1-42). *AIP Advances* **2015**, *5* (9). DOI: 10.1063/1.4921071 (acccessed 3/29/2024).

(22) Nichols, M. R.; Colvin, B. A.; Hood, E. A.; Paranjape, G. S.; Osborn, D. C.; Terrill-Usery, S. E. Biophysical Comparison of Soluble Amyloid-β(1–42) Protofibrils, Oligomers, and Protofilaments. *Biochemistry* **2015**, *54* (13), 2193-2204. DOI: 10.1021/bi500957g.

(23) Hoshino, M. Fibril formation from the amyloid-β peptide is governed by a dynamic equilibrium involving association and dissociation of the monomer. *Biophysical Reviews* **2017**, *9* (1), 9-16. DOI: 10.1007/s12551-016-0217-7.

(24) Morel, B.; Carrasco, M. P.; Jurado, S.; Marco, C.; Conejero-Lara, F. Dynamic micellar oligomers of amyloid beta peptides play a crucial role in their aggregation mechanisms. *Physical Chemistry Chemical Physics* **2018**, *20* (31), 20597-20614, 10.1039/C8CP02685H. DOI: 10.1039/C8CP02685H.

(25) Jin, S.; Kedia, N.; Illes-Toth, E.; Haralampiev, I.; Prisner, S.; Herrmann, A.; Wanker, E. E.; Bieschke, J. Amyloid-β42 Aggregation Initiates Its Cellular Uptake and Cytotoxicity. *Journal of Biological Chemistry* **2016**, *291* (37), 19590-19606. DOI: 10.1074/jbc.M115.691840 (acccessed 2024/03/29).

(26) El-Agnaf, O. M. A.; Mahil, D. S.; Patel, B. P.; Austen, B. M. Oligomerization and Toxicity of β-Amyloid-42 Implicated in Alzheimer's Disease. *Biochemical and Biophysical Research Communications* **2000**, *273* (3), 1003-1007. DOI: https://doi.org/10.1006/bbrc.2000.3051.

(27) Huang, Y.-r.; Liu, R.-t. The Toxicity and Polymorphism of β-Amyloid Oligomers. *International Journal of Molecular Sciences* **2020**, *21* (12), 4477.

(28) Reitz, C. Alzheimer's Disease and the Amyloid Cascade Hypothesis: A Critical Review. *International Journal of Alzheimer's Disease* **2012**, *2012*, 369808. DOI: 10.1155/2012/369808.

(29) Stöhr, J.; Watts, J. C.; Mensinger, Z. L.; Oehler, A.; Grillo, S. K.; DeArmond, S. J.; Prusiner, S. B.; Giles, K. Purified and synthetic Alzheimer's amyloid beta (Aβ) prions. *Proceedings of the National Academy of Sciences* **2012**, *109* (27), 11025-11030. DOI: doi:10.1073/pnas.1206555109.

(30) Sulatskaya, A. I.; Lavysh, A. V.; Maskevich, A. A.; Kuznetsova, I. M.; Turoverov, K. K. Thioflavin T fluoresces as excimer in highly concentrated aqueous solutions and as monomer being incorporated in amyloid fibrils. *Scientific Reports* **2017**, *7* (1), 2146. DOI: 10.1038/s41598-017-02237-7.

(31) Wang, L.; Eom, K.; Kwon, T. Different Aggregation Pathways and Structures for Aβ40 and Aβ42 Peptides. In *Biomolecules*, 2021; Vol. 11.

(32) Bartolini, M.; Naldi, M.; Fiori, J.; Valle, F.; Biscarini, F.; Nicolau, D. V.; Andrisano, V. Kinetic characterization of amyloid-beta 1–42 aggregation with a multimethodological approach. *Analytical Biochemistry* **2011**, *414* (2), 215-225. DOI: https://doi.org/10.1016/j.ab.2011.03.020.

(33) Nirmalraj, P. N.; List, J.; Battacharya, S.; Howe, G.; Xu, L.; Thompson, D.; Mayer, M. Complete aggregation pathway of amyloid β (1-40) and (1-42) resolved on an atomically clean interface. *Science Advances* **2020**, *6* (15), eaaz6014. DOI: doi:10.1126/sciadv.aaz6014.

(34) Linse, S. Mechanism of amyloid protein aggregation and the role of inhibitors. *Pure and Applied Chemistry* **2019**, *91* (2), 211-229. DOI: doi:10.1515/pac-2018-1017 (acccessed 2024-03-20).

(35) Srivastava, A. K.; Pittman, J. M.; Zerweck, J.; Venkata, B. S.; Moore, P. C.; Sachleben, J. R.; Meredith, S. C. β-Amyloid aggregation and heterogeneous nucleation. *Protein Science* **2019**, *28* (9), 1567-1581. DOI: https://doi.org/10.1002/pro.3674.

(36) Sonar, K.; Mancera, R. L. Characterization of the Conformations of Amyloid Beta 42 in Solution That May Mediate Its Initial Hydrophobic Aggregation. *The Journal of Physical Chemistry B* **2022**, *126* (40), 7916-7933. DOI: 10.1021/acs.jpcb.2c04743.

(37) Biancalana, M.; Makabe, K.; Koide, S. Minimalist design of water-soluble cross-β architecture. *Proceedings of the National Academy of Sciences* **2010**, *107* (8), 3469-3474. DOI: doi:10.1073/pnas.0912654107.

(38) Vahdat, A. *The Importance of Macrophages, Lipid Membranes and Seeding in Experimental AA Amyloidosis*; 2019. DOI: 10.3384/diss.diva-159658.

(39) Chen, G.-f.; Xu, T.-h.; Yan, Y.; Zhou, Y.-r.; Jiang, Y.; Melcher, K.; Xu, H. E. Amyloid beta: structure, biology and structure-based therapeutic development. *Acta Pharmacologica Sinica* **2017**, *38* (9), 1205-1235. DOI: 10.1038/aps.2017.28.

(40) Lührs, T.; Ritter, C.; Adrian, M.; Riek-Loher, D.; Bohrmann, B.; Döbeli, H.; Schubert, D.; Riek, R. 3D structure of Alzheimer's amyloid-β(1–42) fibrils. *Proceedings of the National Academy of Sciences* **2005**, *102* (48), 17342-17347. DOI: 10.1073/pnas.0506723102 (acccessed 2024/04/02).

(41) Tian, Y.; Viles, J. H. pH Dependence of Amyloid-β Fibril Assembly Kinetics: Unravelling the Microscopic Molecular Processes. *Angew Chem Int Ed Engl* **2022**, *61* (48), e202210675. DOI: 10.1002/anie.202210675 From NLM.

(42) Kobayashi, S.; Tanaka, Y.; Kiyono, M.; Chino, M.; Chikuma, T.; Hoshi, K.; Ikeshima, H. Dependence pH and proposed mechanism for aggregation of Alzheimer's disease-related amyloid-β(1–42) protein. *Journal of Molecular Structure* **2015**, *1094*, 109-117. DOI: https://doi.org/10.1016/j.molstruc.2015.03.023.

(43) Lee, M.; Kim, J. I.; Na, S.; Eom, K. Metal ions affect the formation and stability of amyloid β aggregates at multiple length scales. *Physical Chemistry Chemical Physics* **2018**, *20* (13), 8951-8961, 10.1039/C7CP05072K. DOI: 10.1039/C7CP05072K.

(44) Abelein, A. Metal Binding of Alzheimer's Amyloid-β and Its Effect on Peptide Self-Assembly. *Accounts of Chemical Research* **2023**, *56* (19), 2653-2663. DOI: 10.1021/acs.accounts.3c00370.

(45) Smith, D. G.; Cappai, R.; Barnham, K. J. The redox chemistry of the Alzheimer's disease amyloid β peptide. *Biochimica et Biophysica Acta (BBA) - Biomembranes* **2007**, *1768* (8), 1976-1990. DOI: https://doi.org/10.1016/j.bbamem.2007.02.002.

(46) Irie, Y.; Keung, W. M. Metallothionein-III Antagonizes the Neurotoxic and Neurotrophic Effects of Amyloid β Peptides. *Biochemical and Biophysical Research Communications* **2001**, *282* (2), 416-420. DOI: https://doi.org/10.1006/bbrc.2001.4594.

(47) Gamberger, D.; Lavrač, N.; Srivatsa, S.; Tanzi, R. E.; Doraiswamy, P. M. Identification of clusters of rapid and slow decliners among subjects at risk for Alzheimer's disease. *Scientific Reports* **2017**, *7* (1), 6763. DOI: 10.1038/s41598-017-06624-y.

(48) Thalhauser, C. J.; Komarova, N. L. Alzheimer's disease: rapid and slow progression. *J R Soc Interface* **2012**, *9* (66), 119-126. DOI: 10.1098/rsif.2011.0134 From NLM.

(49) Falvo, E.; Tremante, E.; Arcovito, A.; Papi, M.; Elad, N.; Boffi, A.; Morea, V.; Conti, G.; Toffoli, G.; Fracasso, G.; et al. Improved doxorubicin encapsulation and pharmacokinetics of ferritin-fusion protein nanocarriers bearing PAS elements. *Biomacromolecules* **2015**, *17*. DOI: 10.1021/acs.biomac.5b01446.

(50) Gremer, L.; Schölzel, D.; Schenk, C.; Reinartz, E.; Labahn, J.; Ravelli, R. B. G.; Tusche, M.; Lopez-Iglesias, C.; Hoyer, W.; Heise, H.; et al. Fibril structure of amyloid-β(1-42) by cryo-electron microscopy. *Science* **2017**, *358* (6359), 116-119. DOI: 10.1126/science.aao2825 From NLM.

(51) Zheng, Y.; Xu, L.; Yang, J.; Peng, X.; Wang, H.; Yu, N.; Hua, Y.; Zhao, J.; He, J.; Hong, T. The effects of fluorescent labels on Aβ42 aggregation detected by fluorescence correlation spectroscopy. *Biopolymers* **2018**, *109* (11), e23237. DOI: https://doi.org/10.1002/bip.23237 (acccessed 2024/03/29).

(52) Hane, F.; Leonenko, Z. Effect of metals on kinetic pathways of amyloid-β aggregation. *Biomolecules* **2014**, *4* (1), 101-116. DOI: 10.3390/biom4010101 From NLM.

(53) Meloni, G.; Sonois, V.; Delaine, T.; Guilloreau, L.; Gillet, A.; Teissié, J.; Faller, P.; Vašák, M. Metal swap between Zn7-metallothionein-3 and amyloid-β–Cu protects against amyloid-β toxicity. *Nature Chemical Biology* **2008**, *4* (6), 366-372. DOI: 10.1038/nchembio.89.

(54) Pedersen, J. T.; Østergaard, J.; Rozlosnik, N.; Gammelgaard, B.; Heegaard, N. H. Cu(II) mediates kinetically distinct, non-amyloidogenic aggregation of amyloid-beta peptides. *J Biol Chem* **2011**, *286* (30), 26952-26963. DOI: 10.1074/jbc.M111.220863 From NLM.

(55) Tran, J.; Chang, D.; Hsu, F.; Wang, H.; Guo, Z. Cross-seeding between Aβ40 and Aβ42 in Alzheimer's disease. *FEBS letters* **2016**, *591*. DOI: 10.1002/1873-3468.12526.

(56) Thacker, D.; Barghouth, M.; Bless, M.; Zhang, E.; Linse, S. Direct observation of secondary nucleation along the fibril surface of the amyloid β42 peptide. *Proceedings of the National Academy of Sciences* **2023**, *120* (25), e2220664120. DOI: doi:10.1073/pnas.2220664120.